Journal of Theoretical Biology 480 (2019) 229–240

Contents lists available at ScienceDirect

Journal of Theoretical Biology

journal homepage: www.elsevier.com/locate/jtb

A multiscale *in silico* model of endothelial to mesenchymal transformation in a tumor microenvironment

M. Chowkwale[a], G.J. Mahler[a], P. Huang[b], B.T. Murray[b,*]

[a] Department of Biomedical Engineering, Binghamton University, PO Box 6000, Binghamton, NY 13902, USA
[b] Department of Mechanical Engineering, Binghamton University, PO Box 6000, Binghamton, NY 13902, USA

ARTICLE INFO

Article history:
Received 26 December 2018
Revised 1 August 2019
Accepted 16 August 2019
Available online 17 August 2019

Keywords:
Cellular potts model
CompuCell3D
EndMT
Cancer metastasis
Mechanobiology
Continuum Model

ABSTRACT

Endothelial to mesenchymal transformation (EndMT) is a process in which endothelial cells gain a mesenchymal-like phenotype in response to mechanobiological signals that results in the remodeling or repair of underlying tissue. While initially associated with embryonic development, this process has since been shown to occur in adult tissue remodeling including wound healing, fibrosis, and cancer. In an attempt to understand the role of EndMT in cancer progression and metastasis, we present a multiscale, three-dimensional, *in silico* model. The model couples tissue level phenomena such as extracellular matrix remodeling, cellular level phenomena such as migration and proliferation, and chemical transport in the tumor microenvironment to mimic *in vitro* tissue models of the cancer microenvironment. The model is used to study the presence of EndMT-derived activated fibroblasts (EDAFs) and varying substrate stiffness on tumor cell migration and proliferation. The simulations accurately model the behavior of tumor cells under given conditions. The presence of EDAFs and/or an increase in substrate stiffness resulted in an increase in tumor cell activity. This model lays the foundation of further studies of EDAFs in a tumor microenvironment on a cellular and subcellular physiological level.

1. Introduction

Endothelial to mesenchymal transformation (EndMT) is a change in endothelial cell phenotype that can occur in response to mechanobiological and biochemical cues, including exposure to inflammatory conditions, abnormal shear stress, mechanical deformation, and abnormal extracellular matrix (ECM) composition (Dahal et al., 2017). This entails a remodeling of the underlying tissue, which is brought about by mesenchymally transformed cells (Dahal et al., 2017; Pardali et al., 2017). These cells give rise to EndMT-derived activated fibroblasts (EDAFs) (Dahal et al., 2017; Pardali et al., 2017; Potenta et al., 2008), which play a role in embryonic development, and adult tissue remodeling such as wound healing, cardiac fibrosis, and cancer (Potenta et al., 2008). EndMT is induced in response to injury to the subendothelial tissue, or inflammatory signals like transforming growth factor-beta (TGF-β) from the surrounding tissue. As shown in Fig. 1, this leads to delamination of endothelial cells from the cell monolayer and loss of cell-cell junctions, as a consequence of the decrease in endothelial cell markers such as vascular endothelial cadherin (VE-cadherin) and platelet endothelial cell adhesion marker 1 (PECAM-1) (Dahal et al., 2017). The cells gain migratory and invasive properties, along with mesenchymal markers, such as alpha-smooth muscle actin (α-SMA) and fibroblast-specific protein 1 (FSP-1) (Potenta et al., 2008).

In a tumor microenvironment, EDAFs can contribute up to 40% of the cancer-associated fibroblast (CAF) population (Potenta et al., 2008). CAFs constitute a majority of the stromal cells in the microenvironment (Yeon et al., 2018), and are known to play a role in metastasis and tumor progression. These fibroblasts secrete ECM proteins, cytokines, and growth factors, which remodel the microenvironment (Potenta et al., 2008; Kalli and Stylianopoulos, 2018). These changes in the tumor microenvironment increase ECM stiffness, inducing activation of fibroblasts and their subsequent migration (Kalli and Stylianopoulos, 2018). The interactions between CAFs and cancer cells determine the extent of metastatic spread (Bendas and Borsig, 2012). Inhibition of these interactions can be a therapeutic target for preventing cancer metastasis. Studying these mechanobiological effects of CAFs, along with the phenomena that occurs in EndMT, requires the integration of models involving different temporal and spatial scales. Today, multiscale, *in silico* models are capable of representing biological and mechanical behavior of such phenomena (Shirinifard et al., 2009; Kleinstreuer et al., 2013; Bailey et al., 2009; Hutson et al., 2017; Lee et al., 2011; Virgilio et al., 2015; Oden et al., 2016).

* Corresponding author.
E-mail address: bmurray@binghamton.edu (B.T. Murray).

https://doi.org/10.1016/j.jtbi.2019.08.012
0022-5193/

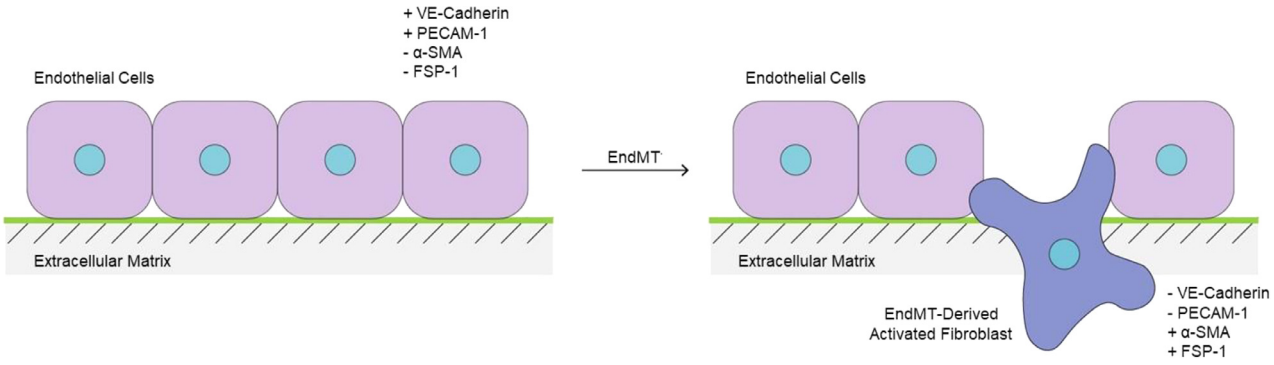

Fig. 1. Schematic of endothelial cells transforming to EndMT-derived activated fibroblasts (EDAFs). The changes in expressed factors in each phase of the process, i.e. endothelial cell markers such as vascular endothelial cadherin (VE-cadherin) and platelet and endothelial cell adhesion molecule 1 (PECAM-1) and mesenchymal cell markers such as alpha-smooth muscle actin (α-SMA) and fibroblast specific protein 1 (FSP-1), are listed. Print in color. (For interpretation of the references to color in this figure legend, the reader is referred to the web version of this article.).

Computational and mathematical models of biological processes have proven to be translational in that they enable the study of development and pathologies at various physical scales (An et al., 2009). Multiscale models incorporate knowledge about physiological and biochemical phenomena at each level to provide a holistic understanding. Agent-based modeling is a cell-based, *in silico* modeling approach which allows the modeling of individual system components and their interactions, in order to simulate cellular behavior observed *in vitro* models. In contrast to the discrete-time and discrete-event approach of agent-based models, continuum models provide a framework to study chemical transport and other physical processes that are coupled to the aforementioned system components. The formulation of continuum models generally leads to a system of coupled partial differential equations, and is well-suited to modeling on the microscale and above (Cristini and Lowengrub, 2010). Combining the two modeling techniques gives rise to hybrid continuum-discrete models which provide the means to study mechanobiology on multiple scales and to account for the interactions between the scales (cells, tissue, etc.). This methodology is especially useful for modeling diseases like cancer, as it requires the handling of intra- and extracellular factors that act on various temporal and spatial scales (Rejniak and Anderson, 2011). One of the most widely used agent-based modeling methods is the cellular Potts model (CPM) (Glazier and Graner, 1993; Szabó and Merks, 2013; Balter et al., 2007). This methodology is implemented in CompuCell3D, a modeling environment for running virtual tissue simulations (Swat et al., 2012). In this method, cell behavior and dynamics are represented in terms of Hamiltonian energy function terms. (Glazier and Graner, 1993). This modeling approach has been validated thoroughly through the simulation of physiological processes and diseases such as vasculogenesis, angiogenesis, tumor evolution and metastasis, embryonic development, cellular transformation, cytokine dynamics in arthritis, and polycystic kidney disease (Kleinstreuer et al., 2013; Szabó and Merks, 2013; Hutson et al., 2017; Abdulla, 2013; Tang et al., 2014; Sluka et al., 2016; Popławski et al., 2009; Belmonte et al., 2016; Baker, 2015). Several computational models exist for epithelial to mesenchymal transformation (EMT), which is a well-studied process similar to EndMT in that epithelial cells undergo a structural and functional change to a mesenchymal phenotype. While both processes are observed in heart development, differences in the processes stem from the distinct sources of the cell. Epithelial cells are derived from the endoderm while endothelial cells are derived from the mesoderm. This results in varying molecular mechanisms, but while the mechanisms of EMT are well documented, those of EndMT are still relatively unknown (Saito, 2013). A hybrid discrete-continuum model simulated EMT using CompuCell3D and found that the loss of endocardial cushion alone does not induce EMT (Abdulla, 2013). Another research group developed a framework based on the differential adhesion hypothesis and used that to simulate EMT and its role in forming cardiac cushions (Neagu et al., 2010). Marin-Riera et al. (2016) developed a rule-based model to simulate EMT in embryonic development (Marin-Riera et al., 2016). This model implements a complete set of basic cell behavior in development. Another model used ordinary differential equations to describe the protein-protein interactions and gene regulatory behavior of EMT (Gould et al., 2016). Here, we present a novel application of CompuCell3D to model cell behavior related to EndMT. The aim of the model is to simulate recent *in vitro* experiments (Mina et al., 2017), to study the interactions between EndMT-derived activated fibroblasts and cancer cells, and to elucidate the effect of EDAFs on tumor progression and metastasis. To the best of our knowledge, this is the first hybrid discrete-continuum model of EndMT which incorporates various physiological levels and uses the Cellular Potts Model.

2. Methods

The simulated cell behavior is based on the Cellular Potts Model (CPM), which is a lattice-based, multi-cell, stochastic methodology for tissue representation. Biological cells are treated as discrete entities, each with characteristic values of volume, surface area, and intrinsic motility on a regular lattice. In the present implementation, the cells interact with each other and the surrounding extracellular matrix (ECM) via adhesion, secretion of factors, and cell migration. A series of reaction-diffusion and steady-state equations are used to describe the transport of chemical fields that diffuse through the system, such as oxygen, carbon dioxide, cytokines, matrix degrading enzymes, and extracellular matrix proteins. Oxygen acts as the growth-limiting nutrient; cell growth and proliferation depends on the amount of oxygen available to the cells. Carbon dioxide is secreted by the cells as a waste product. Cytokines are introduced in the model to represent the onset of inflammation, and play a role in the activation of the cells. Specific assumptions include: (a) Inflammation is introduced by randomly placing an EndMT-derived activated fibroblast in the endothelial monolayer. (b) The amount of carbon dioxide secreted by the cells is equal to the amount of oxygen consumed by the cells. (c) The removal of carbon dioxide occurs at a rate that is twice the rate of the natural decay of oxygen. (d) The rate of chemical production or consumption of quiescent cells is half the rate for proliferating cells. Assumption (a) was made to allow for physiologically relevant cytokine levels to be introduced into the system. Assumptions (b) and (c) were made due to the lack of

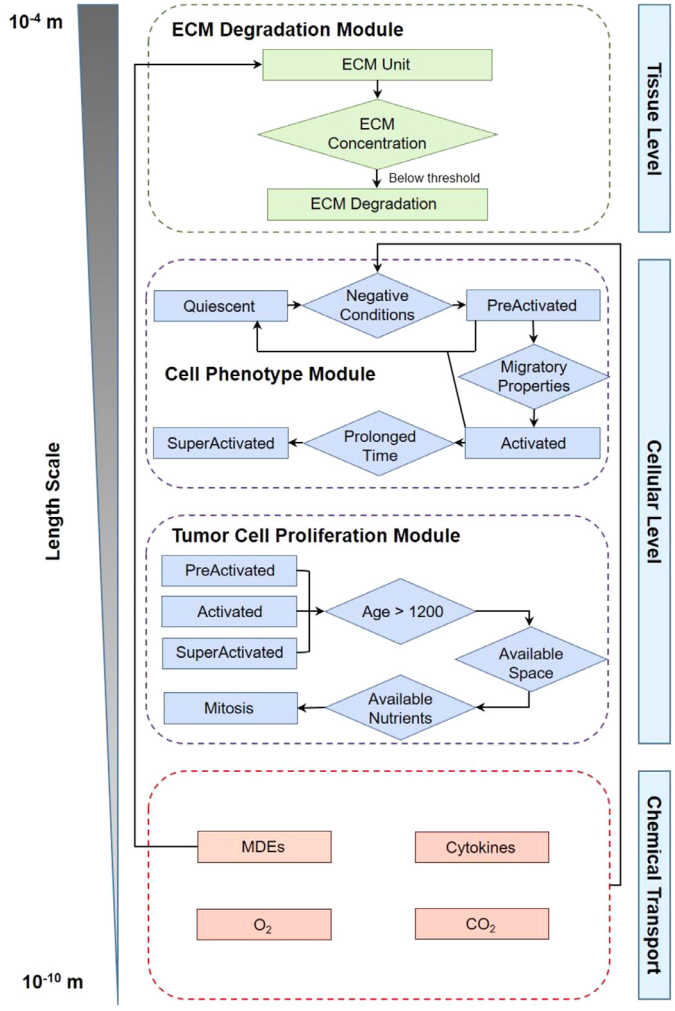

Fig. 2. Multiscale structure of the computational model. The extracellular matrix (ECM) degradation module shows degradation of ECM due to the presence of matrix degrading enzymes (MDEs). The Cell Phenotype module shows a generalized schematic for phenotype changes of endothelial and tumor cells. The Tumor Cell Proliferation module outlines the conditions required for tumor cell mitosis. The last block represents the chemical fields in the continuum transport model. Print in color. (For interpretation of the references to color in this figure legend, the reader is referred to the web version of this article.).

waste secretion rates available in primary literature. Assumption (d) simplifies the metabolic differences between quiescent and proliferating cells (Wagner et al., 2011; Swat et al., 2015). The overall structure of the model is illustrated in Fig. 2.

In the CPM, the cells are individual voxels or clusters of voxels on a fixed cell lattice, where each voxel has a position $\vec{x}$ and an index $\sigma(\vec{x})$ associated with it. Each cell behavior is associated with an effective energy term, which is a representation to produce desired actions and not related to an actual physical energy. For example, modeling a cell with a defined volume v and surface area s requires two effective energy terms for cell-volume and cell-surface constraints, shown in the first and second terms of the following equation, respectively:

$$H = \sum_{\sigma} \lambda_V (v - V_T)^2 + \sum_{\sigma} \lambda_S (s - S_T)^2 \quad (1)$$

where λ_V and λ_S are constraint strengths that represent the elastic modulus of the cells (Swat et al., 2015), V_T is the target volume, and S_T is the target surface area. The algorithm performs a series of voxel-copy attempts, where neighboring lattice sites are selected as the target and source site. The change in effective energy that occurs if the index of the source-site voxel is copied to the target-site voxel is calculated. The CPM voxel-copy mechanism aims to lower the effective energy change of the simulation, and the configuration which allows this is selected for the next series of attempts. One set of voxel-copy attempts occurs in one unit of simulation time, which is known as a Monte Carlo Step (MCS). The number of voxel-copy attempts is dependent on the number of voxels in the cell lattice. The spatial resolution of the model is dependent on the size of the cell-lattice voxel. In physiologically-relevant simulations, the MCS and experimental time are proportional, and the spatial resolution follows a metric scale.

Table 1
CompuCell3D parameters.

CompuCell3D Parameter	Value
Temperature	5
Voxel (side)	10 μm
Voxel (volume)	1000 μm^3
Monte Carlo Step	60 s
Lattice dimensions	100×100×100 voxels
Target cell volume	2
Target cell surface area	8
Lambda volume for cells	156
Lambda surface for cells	156
Lambda chemotaxis for quiescent cells	200
Lambda chemotaxis for proliferating cells	100

In this study, three main generalized cell classes are defined: tumor cells, endothelial cells, and ECM. The tumor cells have three subtypes: quiescent cancer cells, activated cancer cells, and metastatic cancer cells. Similarly, endothelial cells have three subtypes: quiescent endothelial cells, EndMT-derived activated fibroblasts (EDAFs), and superactivated EDAFs. The ECM is represented as a uniform medium. CompuCell3D cell types are used to define each of these cell types, ECM, and a default cell type called Medium, which represents the extracellular space. Based on the number of cells used in the *in vitro* tissue model, for the simulations, the initial cell counts are 10,000 for endothelial cells and 500,000 for tumor cells. Each cell is initially set as a voxel. As cell diameter is approximately 10 μm, each voxel edge corresponds to 10 μm in real-world units. Furthermore, the experimental endothelial cell-migration speed is ~0.3 μm/min (Kick et al., 2016), and the experimental cancer cell-migration speed ranges from 0.14 μm/min to 0.3 μm/min (Kikuchi et al., 2011; Truong et al., 2016). To match the experimental cell speeds to the simulated cell speeds, one MCS was set to one minute. A temperature parameter was used to prescribe the entropy of the stochastic cell migration, and it is not representative of the physical temperature. It should be noted that the use of small target volumes is generally unsuitable for such simulations, as the cells can obtain a volume of zero and disappear. However, CompuCell3D provides mathematical constraints for calculating lambda values, temperature, and target values in such a manner that disappearance does not occur (Swat et al., 2013). We have calculated the parameter values based on these constraints, and then tested them to ensure that they resulted in a stable simulation. For the values used in the simulations, cell disappearance did not occur. The CompuCell3D parameters are summarized in Table 1.

Cells attach to other cells and the extracellular matrix through cell-surface proteins, such as cadherins and integrins (Alberts et al., 2002). A possible theory for cadherin-mediated cell-cell adhesion is based on homolytic binding, where molecules on one cell bind with the same type of molecules on another cell (Alberts et al., 2002). Integrins act as matrix receptors and bind to many ECM proteins such as collagen, fibronectin, and laminins (Alberts et al., 2002). CompuCell3D simulates cell adhesion using contact energies, which essentially represent the adhesion bond strength

Table 2
Contact energies between the different cell types. Med = Medium, ECM = extracellular matrix, QE = quiescent endothelial cells, PE = preactivated endothelial cells, AE = EndMT-derived activated fibroblasts (EDAF), SE = superactivated EDAFs, QT = quiescent tumor cells, PT = preactivated tumor cells, AT = activated tumor cells, and ST = superactivated tumor cells.

	Med	ECM	QE	PE	AE	SE	QT	PT	AT	ST
Med	20	20	20	20	20	20	20	20	20	20
ECM		15	5	5	5	5	5	5	5	5
QE			3	3	3	3	3	3	3	3
PE				3	3	3	3	3	3	3
AE					3	3	3	3	3	3
SE						3	3	3	3	3
QT							3	3	3	3
PT								3	3	3
AT									3	3
ST										3

between cells. The effective energy term for contact energy in a three-dimensional model is,

$$H = \sum_{i,j,neighbors} J\left(\tau_{\sigma(i)},\ \tau_{\sigma(j)}\right)\left(1 - \delta_{\sigma(i),\sigma(j)}\right) \tag{2}$$

where J is the contact energy per unit area, τ is the cell type, i and j are indices of neighboring lattice sites, and $\delta_{\sigma(i),\sigma(j)}$ is the Kronecker delta function. The factor $(1 - \delta_{\sigma(i),\sigma(j)})$ ensures that voxels of different cell types are being compared. However, the value of the contact energy is not as important to the model as the hierarchy of contact energies between cells (Swat et al., 2012). We make the assumption that endothelial cells and cancer cells bind to cells of the same type and each other more strongly than they bind to ECM. Consequently, the contact energy hierarchy for our model is as follows:

$$\begin{aligned} J_{endothelial,\,endothelial} = J_{endothelial,\,cancer} = J_{cancer,\,cancer} \ > \ J_{endothelial,\,ECM} \\ = J_{cancer,\,ECM} > J_{ECM,\,ECM} \end{aligned} \tag{3}$$

Based on this hierarchy and the mathematical constraints stated in the CompuCell3D Quick Start Guide (Version 3.7.0) (Swat et al., 2013), different contact energy values were tested to observe the resulting cell speeds. The contact energies presented in Table 2 were used in the model as they resulted in a range of cell speeds that matched experimentally observed cell speeds.

Cytoskeleton-dependent phenomena, such as protrusion, attachment, and traction, result in cell motility (Alberts et al., 2002). While random motility is promoted in mammalian cells in the absence of an extracellular stimulus (Kölsch et al., 2008), gradients of diffusible chemicals, substrate stiffness, and cell adhesion result in directional movement of cells (Alberts et al., 2002; Wen et al., 2015). The directed migration of cancer cells in the tumor microenvironment plays a substantial role in cancer metastasis (Roussos et al., 2011). Tumor cells invade in the direction of the nutrient source (Kenney et al., 2016) and higher concentrations of inflammatory cytokines (Mandel et al., 2013). Moreover, the tumor cell migration speed increases with an increase in endothelial cell invasion into the ECM (Mina et al., 2017). While the dynamic motility in the model is intrinsically simulated in the voxel-copy attempts (Swat et al., 2012), the chemotactic behavior of the cells was represented in terms of the effective energy term,

$$H = \lambda_{chem}\ (c(x_{destination}) - c(x_{source})) \tag{4}$$

where λ_{chem} is a constraint representing the extent to which the difference in chemical concentrations will affect chemotaxis, and $c(x_{destination})$ and $c(x_{source})$ represent the chemical concentrations at the source and potential destination voxels in the cell lattice. This equation is used to model chemotaxis of tumor cells towards higher oxygen and cytokine concentrations and haptotaxis of endothelial cells towards higher concentrations of ECM proteins.

Nutrient and waste concentrations in tissues are maintained in normal ranges by blood vessels through constant supply and removal, respectively. Oxygen and carbon dioxide are used in the model to represent the nutrient and waste concentrations. They diffuse through tissue rapidly, and therefore can be modeled using a steady-state diffusion equation (Popel, 1989). CompuCell3D uses the Helmholtz equation to solve for steady-state diffusion concentrations.

$$\nabla^2 X - \lambda X = F \tag{5}$$

Here X is the chemical concentration, λ is the natural decay rate of the chemical field, and F is a function which models the secretion and uptake of the chemical by the cells. The function for oxygen includes the oxygen source and consumption of oxygen by the cells, while secretion is represented in the equation for carbon dioxide. As there is a constant nutrient source in the model, the oxygen diffusion model uses Dirichlet boundary conditions along the y-axis; the y-minimum condition is zero and the y-maximum condition is set to 10^{-15} moles. Similarly, the carbon dioxide diffusion model implements the y-minimum and the y-maximum derivative (Neumann) boundary conditions set equal to zero to represent no flux of carbon dioxide at the boundaries of the system, which is what occurs *in vitro* setups. These values were determined based on experimental data to ensure that the virtual tissue has physiologically-relevant partial pressures of oxygen and carbon dioxide as shown in Table 3. Zero derivative boundary conditions along the x- and z-axes are used for both chemical species.

Mediators of inflammation that induce endothelial fibrosis are transforming growth factor-beta (TGF-β), interleukin-1 (IL-1), tumor necrosis factor-alpha (TNF-α), bacterial endotoxins, and oxidative stress (Pérez et al., 2017; Cho et al., 2018). Some of these factors trigger EndMT, and lead to the transformation of endothelial cells to EndMT-derived activated fibroblasts (Mahler et al., 2013). Consequently, cytokine diffusion throughout the tissue is also a component of the continuum transport model. The cytokines are introduced to the model by randomly placing an EDAF in the endothelial monolayer. The rate of change of cytokine concentration C is governed by the following reaction-diffusion equation:

$$\partial C/\partial t = D_{IC}\ \nabla^2 C + \beta c - \gamma C \tag{6}$$

where D_{IC} is the diffusion coefficient of the inflammatory cytokines, β is the production rate of inflammatory cytokines by the activated and superactivated tumor cells, EDAFs, and superactivated EDAFs, and γ is the removal of inflammatory cytokines due to natural decay. A similar equation is used to model the behavior of matrix degrading enzymes (MDEs) that are secreted by peripheral tumor cells. MDEs include matrix metalloproteinases (MMPs) and urokinase plasminogen activators (uPAs) and are responsible for ECM degradation. This facilitates ECM remodeling, and promotes tumor cell migration and proliferation (Ramis-Conde et al., 2008). For simplicity, MMPs and uPAs are grouped into a category called MDEs in the *in silico* model (Anderson, 2007). The degradation of extracellular matrix proteins is modeled as,

$$\partial e/\partial t = -\alpha m e \tag{7}$$

Here e is the ECM protein concentration at that lattice site, m is the MDE concentration, and α is the degradation rate of ECM by MDEs. The parameters used in the continuum transport model are summarized in Table 3.

Environmental factors such as a lack of nutrients, increased acidity due to carbon dioxide build-up, and increased exposure to inflammatory conditions result in quiescent cells becoming activated phenotypes (Pérez et al., 2017; Tang et al., 2014). These changes in phenotype can be temporary or permanent, depending on the duration of unfavorable conditions. Our model incorporates low oxygen partial pressures, high carbon dioxide partial pressures, and increased cytokine concentrations as conditions that

Table 3
Physiological values of parameters in the continuum transport model and their adjusted values.

Parameter	Physiological Value	Adjusted Value	References
O_2 partial pressure	38 mmHg	–	(McKeown, 2014; Trepiana et al., 2017; Horsman and Vaupel, 2016)
CO_2 partial pressure	40 mmHg	–	(Markwalder et al., 1984; Arthurs and Sudhakar, 2005)
O_2 consumption rate by tumor cells, ϕ_T	$2 \times 10^{-15} moles/cell/min$	$3.33 \times 10^{-17} moles/cell/MCS$	(Caicedo et al., 2015; Wagner et al., 2011)
O_2 consumption rate by endothelial cells, ϕ_E	17×10^{-18} $moles/cell/s$	$1.02 \times 10^{-15} moles/cell/MCS$	(Wagner et al., 2011), (Usselman et al., 2016)
Natural decay rate of O_2, λ	$0.1\ /min$	$0.1\ /MCS$	(Cristini and Lowengrub, 2010)
CO_2 production rate by tumor cells, δ_T	2×10^{-15} $moles/cell/min$	3.33×10^{-17} $moles/cell/MCS$	Assumption, equivalent to O_2 consumption rate
CO_2 production rate by endothelial cells, δ_E	17×10^{-18} $moles/cell/s$	1.02×10^{-15} $moles/cell/MCS$	Assumption, equivalent to O_2 consumption rate
CO_2 removal from tissue, λ	$0.2\ /min$	$0.2\ /MCS$	Assumption. Assumed to be twice the oxygen decay.
Diffusion coefficient of cytokines, D_{IC}	0.1×10^{-10} m^2/sec	$6\ pixel^2/MCS$	(Eladdadi et al., 2014; Su et al., 2009; Albro et al., 2013; Hao et al., 2017)
Cytokine production rate by tumor cells, β	$1/cell/min$	$1/cell/MCS$	(Eladdadi et al., 2014)
Cytokine natural decay rate, γ	$2\ /day$	$1.38 \times 10^{-3}/MCS$	(Eladdadi et al., 2014; Su et al., 2009)
Diffusion coefficient of MDE, D_m	10^{-9} cm^2/sec	6×10^{-2} $pixel^2/MCS$	(Gerisch and Chaplain, 2008; Nargis et al., 2018; Anderson, 2005)
MDE production rate by tumor cells, β	$0.01\ /s$	$0.6\ /MCS$	(Kumar et al., 2016)
MDE natural decay rate, γ	$0.001\ /s$	6×10^{-2} $/MCS$	Assumption based on Ramis-Conde et al., 2008.
ECM degradation rate by MDE	0.02 /s	1.2 /MCS	Assumption based on Ramis-Conde et al., 2008.

Table 4
Summary of the cell behaviors modeled for each of the cell types.

Cell Types	Modeled Behavior	References
Quiescent Tumor Cells	• Consume oxygen • Secrete carbon dioxide	(Wagner et al., 2011; Swat et al., 2015)
Preactivated, Activated, and Superactivated Tumor Cells	• Consume oxygen • Secrete carbon dioxide • Secrete inflammatory cytokines • Secrete MDEs when in contact with ECM • Chemotaxis towards oxygen and cytokines • Undergo mitosis every 20 h	(Anderson, 2007; Pérez et al., 2017; Tang et al., 2014; Ramis-Conde et al., 2008)
Quiescent Endothelial Cells	• Consume oxygen • Secrete carbon dioxide	(Wagner et al., 2011; Swat et al., 2015)
Preactivated endothelial cells, EndMT-derived activated fibroblasts (EDAFs), and Superactivated EDAFs	• Consume oxygen • Secrete carbon dioxide • Secrete inflammatory cytokines • Chemotaxis towards cytokines	(Pérez et al., 2017; Tang et al., 2014)

cause quiescent cells to gain migratory properties. When the cells have migrated more than 80 μm, they transition to an activated phenotype (Mosadegh et al., 2015). For the purpose of programming simplicity, the former cell types (those that have migrated <80 μm) are represented as preactivated cells. An improvement in these conditions may result in activated cells transitioning back to quiescent cells, when the nutrient, waste, and cytokine levels are in a biologically-favorable range. However, if the activated cells remain in the phenotype for more than 48 h, they transition to a superactivated phenotype, which cannot revert to quiescent cells. To model the metabolism of these cells in a physiologically relevant manner, the rates of oxygen consumption and carbon dioxide secretion of quiescent cells are half the rates for proliferating cells (Wagner et al., 2011; Swat et al., 2015). Similarly, the rates of matrix degrading enzyme secretion and cytokine secretion for preactivated cells are half the rates for activated and superactivated cells. Tumor cell growth and proliferation is based on the cell age and available nutrients and space (Anderson, 2007; Enderling et al., 2009; Swat et al., 2015). As the time taken for each cell cycle is around 20 h (Yu et al., 2001), non-quiescent cells can undergo mitosis if their age is greater than 20 h. This corresponds to 1200 Monte Carlo steps in the model. Another condition for mitosis is the availability of nutrients (oxygen) and space around the dividing cell. Availability of space was determined by checking if there were any endothelial, tumor, or ECM cells around the dividing cell. If all three requirements are fulfilled, the tumor cell can undergo mitosis. As the simulation is run for an equivalent of 48 h in real time, cell proliferation does not reach the Hayflick limit (Rubin, 2002; Hayflick, 1965). The time duration of 48 h was chosen because the *in vitro* experiments from previous studies (Mahler et al., 2013; Dahal et al., 2017; Mina et al., 2017) were performed for the same time interval. Consequently, cell behavior such as cell senescence and death is not relevant, and was not incorporated in the model. The cell behavior modeled for each of the cell types has been summarized in Table 4.

3. Results

The simulations performed on the system illustrate tumor cell behavior in initial diseased states. The simulated behavior was compared with the results from an *in vitro* microfluidic experiment which modeled EndMT in the tumor microenvironment

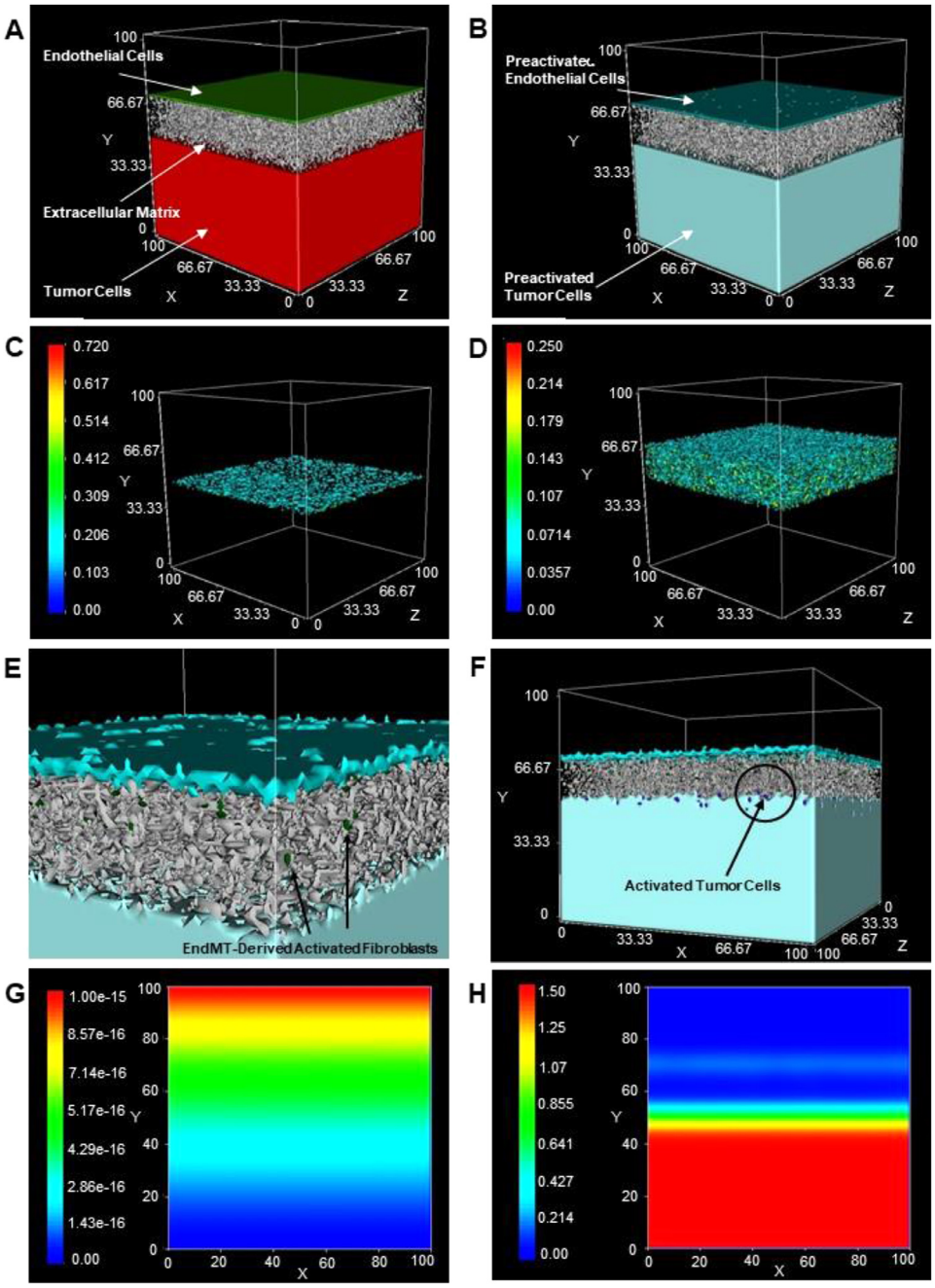

Fig. 3. (A) Simulation snapshot of the initial conditions of the 3D model in CompuCell3D. Green = quiescent endothelial cells. Grey = extracellular matrix (ECM). Red = quiescent tumor cells. (B) Simulation snapshot of the model when all the cells become preactivated due to the cells being subjected to inflammatory conditions. Cyan = preactivated endothelial cells. Light blue = preactivated tumor cells. (C) Presence of matrix degrading enzymes (MDEs) secreted by non-quiescent tumor cells in the 3D model at Monte Carlo step (MCS) = 100. (D) Varying concentration of ECM proteins due to degradation by MDEs at MCS = 100. (E) Zoom-in view of the 3D model to show EndMT-derived activated fibroblasts (EDAFs) (dark green, pointed to with the arrow). (F) Protrusions (highlighted by the circle) and activated tumor cells (purple, pointed to with the arrow) formed due to migration of the tumor cells. (G) Chemical concentration map showing diffusion of oxygen throughout the system. The red portion at $Y = 100$ indicates the highest concentration of oxygen at the source, i.e. the simulated top of a cell culture flask. The oxygen concentration decreases towards the bottom of the system, i.e. towards the tumor cells. (H) Chemical concentration map showing diffusion of cytokines throughout the system. The red portion in the bottom half of the system indicates the presence of the source of cytokine secretion, i.e. the tumor cells. Print in color. (For interpretation of the references to color in this figure legend, the reader is referred to the web version of this article.).

(Mina et al., 2017). Based on the experimental results, it was determined that the distance travelled by tumor cells was consistent across hydrogels with the same stiffness. Moreover, their tissue model had more migration of tumor cells in the presence of EDAFs as compared to the absence of EDAFs which was observed in the in silico model under the highest stiffness. In addition, they observed increased tumor cell proliferation in the presence of EDAFs as compared to the absence of EDAFs. Lastly, these *in vitro* studies showed that there was an increase in tumor cell invasion and proliferation as substrate stiffness increased. An increase in tumor cell activity in response to progressed disease states (represented by increases in substrate stiffness) was observed in the *in silico* model. The effects of the presence of simulated EDAFs on tumor cell behavior were limited. The three-dimensional multiscale model shown in

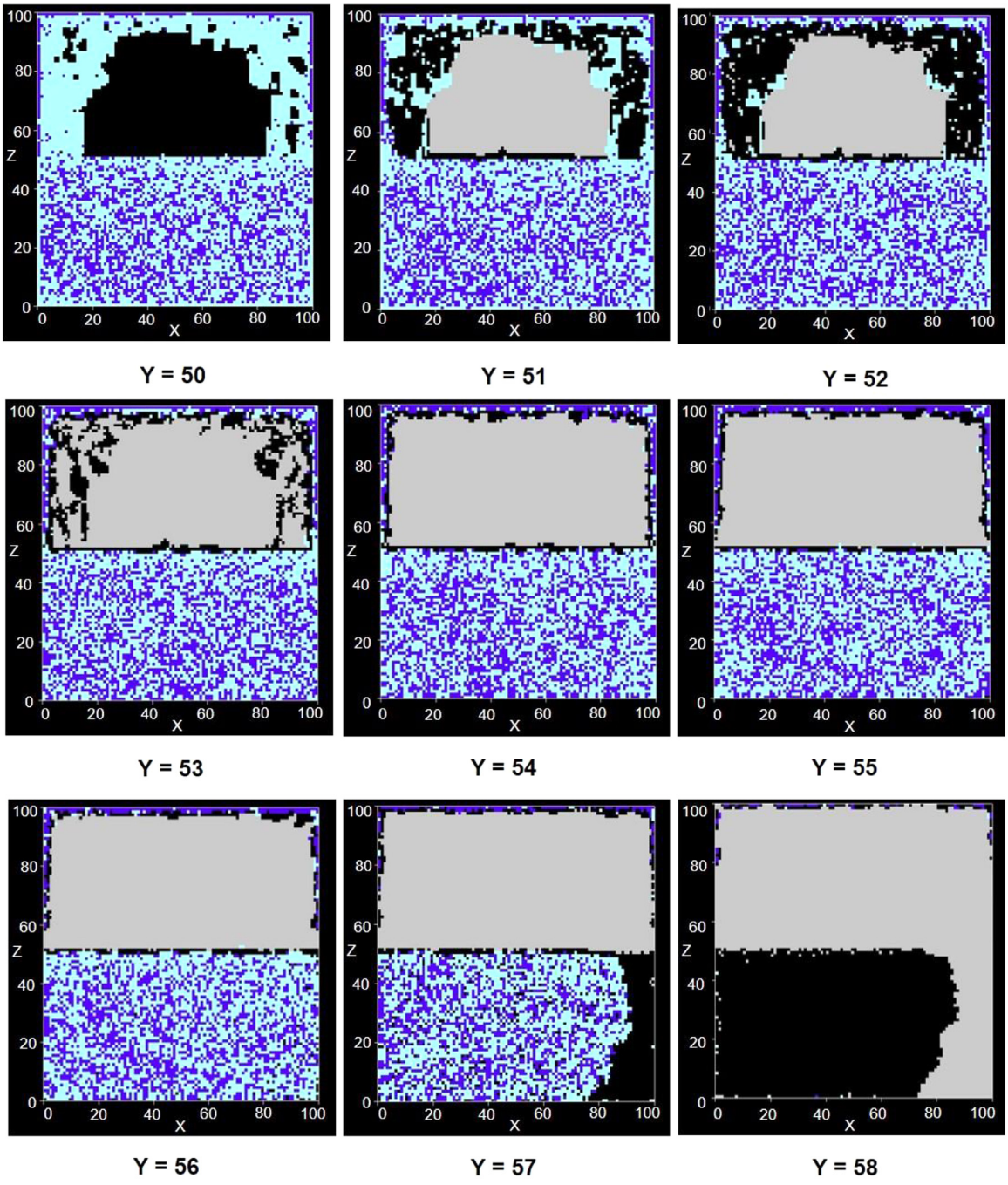

Fig. 4. Degradation of extracellular matrix (ECM) and the protrusion-like growth and migration of tumor cells shown through screenshots of the model along the vertical axis from $Y=50$ to 58. The panel for $Y=50$ shows how the tumor cells have completely degraded the ECM in that plane, while the panels corresponding to $Y=51$, 52, and 53 show varying degradation of ECM due to the surrounding tumor cells. The line present in all images around $Z=50$ is a result of degraded ECM due to the tumor cells. At $Y=58$, the empty section shows ECM degraded by the tumor cells at the tip of the protrusion (in $Y=57$). The purple cells are activated tumor cells, light blue cells are preactivated tumor cells, and grey cells represent ECM. The black areas represent Medium cells which occur due to ECM degradation in the voxel. Print in color. (For interpretation of the references to color in this figure legend, the reader is referred to the web version of this article.).

Fig. 3A is an accurate representation of the *in vitro* tissue model in Mina et al. (2017) Fig. 5A. The computational model also correctly simulates tumor cell behavior in early stages of tumor growth, such as the presence of activated tumor cells and protrusions that occur when metastasis begins (Sai et al., 2016). Fig. 3B shows a snapshot of the model as the cells become preactivated in response to inflammatory conditions. The diffusion of chemical fields occurred in a manner similar to that in an *in vitro* set up, as shown in Fig. 3C, D, G, and H. Fig. 4 shows the degradation of ECM at each y-coordinate between $Y=50$, which is the outermost layer of cells in the tumor spheroid, and $Y=58$, which is the distance to which a protrusion invaded into the surrounding tissue. The panel for $Y=50$ shows how the tumor cells have completely degraded the ECM in that plane, while the panels corresponding to $Y=51$, 52, and 53 show varying degradation of ECM due to the surrounding tumor cells. The line present in all images around $Z=50$ is a result of degraded ECM due to the tumor cells. At $Y=58$, the empty section shows ECM degraded by the tumor cells at the tip

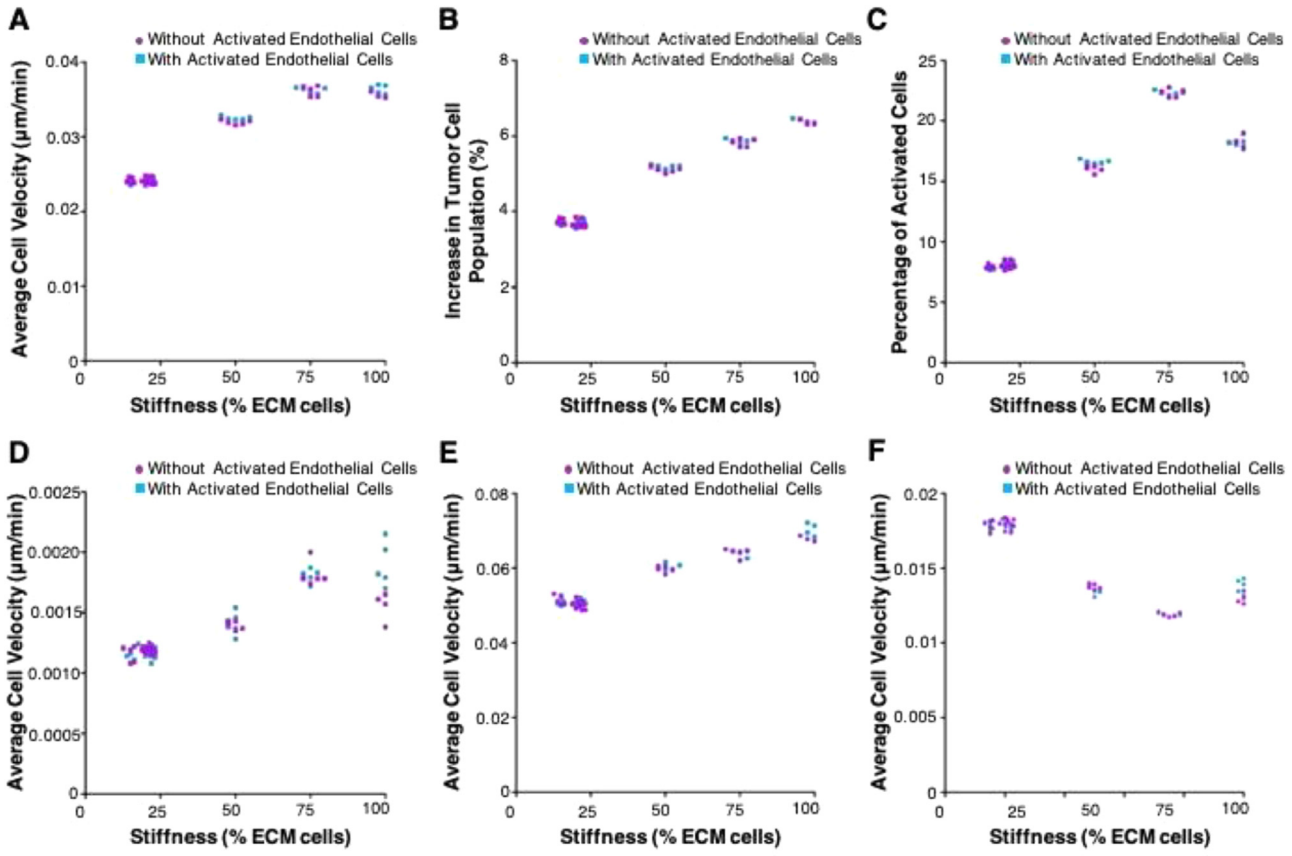

Fig. 5. Scatter plots presenting various metrics of tumor cell behavior in the presence (blue square) and absence (purple circle) of EndMT-derived activated fibroblasts (EDAFs) and varying substrate stiffness at the end of the simulations. The replicates for each condition ($n = 5$ to 7) are plotted in each graph. (A) Average tumor cell velocity increases as substrate stiffness increases from 15% stiffness ECM to 75% stiffness ECM and remains the same at 100% stiffness ECM. (B) Increase in tumor cell population increases with an increase in substrate stiffness. (C) The fraction of activated tumor cells in the tumor cell population increases as substrate stiffness increases from 15% stiffness ECM to 75% stiffness ECM but decreases at 100% stiffness ECM. (D) The velocity of tumor cells in the y-direction, i.e. into the extracellular matrix, increases with an increase in substrate stiffness. The vertical velocity of tumor cells is higher in the presence of EDAFs. (E) The average cell velocity for activated tumor cells increases with an increase in substrate stiffness, with an apparent difference between the two conditions at 100% stiffness ECM. (F) The vertical velocity of activated tumor cells decreases with an increase in substrate stiffness from 15% stiffness ECM to 75% stiffness ECM, but increases at 100% stiffness ECM. There is an apparent difference between the two conditions at 100% stiffness ECM, indicating that the presence of EDAFs in stiff substrates might increase tumor cell migration. Print in color. (For interpretation of the references to color in this figure legend, the reader is referred to the web version of this article.).

of the protrusion (in $Y = 57$). This shows how cells secrete MDEs to degrade the surrounding matrix to make way for cell migration.

3.1. Presence of EndMT-derived activated fibroblasts increases tumor cell activity

In the absence of EDAFs, the average tumor cell velocity (calculated as total displacement of cell divided by the time is possessed migratory properties) was found to be 0.0355 ± 0.00035 μm/min, and the tumor cell population increased by 6.357%. In the simulation, endothelial cells are expected to be activated due to tumor-produced cytokines. However, previous work has shown that small numbers of EndMT-derived activated fibroblasts are found after 48 h in EndMT-promoting conditions (Mahler et al., 2013; Dahal et al., 2017). This process would require a much longer simulation time. Thus, to limit simulation time while determining the effect of EDAFs on tumor cells, EDAFs were embedded in the extracellular matrix. The proportion of EDAFs was set to 5% of the initial endothelial cell population (Wang et al., 2018). In the presence of EDAFs, the average tumor cell speed was 0.0363 ± 0.00057 μm/min, and the increase in tumor cell population was 6.4%. Activated tumor cells constituted 18.314% of the tumor cell population in the absence of EDAFs whereas this percentage became 18.07% in the presence of EDAFs.

3.2. An increase in substrate stiffness increases tumor cell activity

Extracellular matrix stiffness is known to play a role in tumorigenesis (Pathak and Kumar, 2012). To simulate varying stiffness of the extracellular matrix that result from disease progression, a ratio of ECM and Medium type cells was used. A higher ECM concentration (i.e., stiffer substrate) was represented by a higher ratio of ECM cells to Medium cells. As the contact energy between ECM and tumor cells is lower than the contact energy between tumor cells and Medium, contact between ECM and tumor cells is preferred by the algorithm. This results in more ECM-tumor cell adhesion, which in turn allows more guided migration along ECM cells, a commonly observed phenomenon in cell migration studies (Lauffenburger and Horwitz, 1996). Based on the literature review conducted, the highest collagen concentration in a 3D, *in vitro* tumor environment cell culture model hydrogel was 10 mg/ml (Szot et al., 2011). In the model, this was represented as 100% ECM cells and 0% Medium cells. In a similar manner, the collagen concentrations used in our previous *in vitro* experiments - 1.5 mg/ml, 2.0 mg/ml, and 2.2 mg/ml - were represented as 15%, 20%, and 22% ECM cells with the remaining proportions as Medium cells.

As seen in Fig. 5A, the overall velocity of the tumor cells increases from 0.0241 ± 0.00038 μm/min in 15% stiffness to 0.0361 ± 0.00072 μm/min in 75% stiffness ECM cells, but does not change

significantly in 100% stiffness ECM cells in the absence of EDAFs. In the presence of EDAFs, the overall tumor cell velocity increases from 0.0239 ± 0.00042 μm/min in 15% stiffness ECM to 0.0361 ± 0.00043 μm/min in 75% stiffness ECM. A similar trend is followed in Fig. 5D, where the velocity of the cells in the y-direction, i.e. into the hydrogel, increases from 0.00115 ± 6.85E-05 μm/min in 15% stiffness ECM to 0.00181 ± 0.00010 μm/min in 75% stiffness ECM in the absence of EDAFs. In the presence of EDAFs, the velocity in the y-direction increases from 0.00114 ± 4.95E-05 μm/min in 15% stiffness ECM to 0.00180 ± 5.59E-05 μm/min in 75% stiffness ECM. This increase in velocity stems from an increase in the displacement of the cells (which primarily takes place in the y-direction; data not shown), which shows that increased stiffness results in increased cell invasion. In the 100% stiffness ECM condition, the tumor cell velocity in the presence of EDAFs increases to 0.00189 ± 0.00018 μm/min. However, in the absence of EDAFs, the tumor cell velocity decreases from 0.00181 ± 0.00010 μm/min in the 75% stiffness ECM condition to 0.00156 ± 0.00010 μm/min in the 100% stiffness ECM condition. Consequently, the tumor cell velocity in the presence of EDAFs is greater than the tumor cell velocity in the absence of EDAFs. This is not a trend that is apparent in the other stiffness conditions, and can therefore indicate that the presence of EDAFs in a stiff substrate may increase tumor cell migration. The increase in tumor cell population increases from 3.738 ± 0.081% in 15% stiffness ECM to 6.357 ± 0.054% in 100% stiffness ECM in the absence of endothelial cells, and 3.695 ± 0.061% in 15% stiffness ECM to 6.404 ± 0.046% in 100% stiffness ECM in the presence of endothelial cells as shown in Fig. 5B. In Fig. 5C, the percentage of activated tumor cells increases with an increase in substrate stiffness from 7.914 ± 0.11% in 15% stiffness ECM to 22.305 ± 0.38% in 75% stiffness ECM, but decreases to 18.314 ± 0.41% at 100% stiffness ECM in the absence of EDAFs. These numbers do not change significantly in the presence of EDAFs. Fig. 5E and F show how substrate stiffness affects the velocity of activated tumor cells. Fig. 5E shows the overall average velocity of activated tumor cells and Fig. 5F shows the trends of the vertical velocity (i.e. into the hydrogel) of activated tumor cells. The horizontal velocity in the absence of EDAFs increases as substrate stiffness increases from 0.0514 ± 0.0012 μm/min in 15% stiffness ECM to 0.0678 ± 0.00056 μm/min in 100% stiffness ECM, as there is more ECM for the tumor cells to move along. In the presence of EDAFs, the horizontal velocity of activated tumor cells increases from 0.0509 ± 0.0010 μm/min in 15% stiffness ECM to 0.0703 ± 0.0015 μm/min in 100% stiffness ECM. However, there is a decrease in the vertical velocity of the activated tumor cells from 0.0178 ± 0.00036 μm/min in 15% stiffness ECM to 0.0119 ± 0.00015 μm/min in 75% stiffness ECM, but increases to 0.0129 ± 0.00036 μm/min at 100% stiffness ECM in the absence of EDAFs. The same trend is followed in the presence of EDAFs, with the vertical velocity at 100% stiffness ECM being 0.0137 ± 0.00046 μm/min. This could be an outcome of the activated tumor cells' preferred direction of movement being along the orientation of the ECM cells, as opposed to invading into the hydrogel. Furthermore, both the horizontal and vertical velocities at 100% stiffness ECM are higher in the presence of EDAFs than in the absence of EDAFs, indicating that EDAFs can alter tumor cell behavior at higher substrate stiffness. As EDAFs remodel the underlying extracellular matrix, an indirect effect of their presence on tumor cells is seen through the effects of substrate stiffness on tumor cell behavior. However, a direct effect is not as apparent from the modeled EDAF behavior, which is a deviation from the observations in the *in vitro* experiments. This may be due to the unconfined nature of the computational model, which has previously been shown to result in slow tumor cell migration when compared to confined models (Pathak and Kumar, 2012).

4. Discussion

Here we present a novel, multiscale model of EndMT in a tumor microenvironment. The results obtained from the simulations were compared with *in vitro* tissue models of tumor microenvironments. Mina et al. (2017) created a microfluidic device to study EndMT *in vitro*. Using this device, it was determined that the distance travelled by tumor cells was consistent across hydrogels with the same stiffness. Moreover, their model had more migration of tumor cells in the presence of EDAFs as compared to the absence of EDAFs, which is also shown in our *in silico* model. Lastly, Mina et al. saw ∼2.5% proliferation in tumor cells in the 2.2 mg/ml collagen hydrogel without activated fibroblasts, and ∼4% proliferation with activated fibroblasts. However, the distance travelled by the cells in the cell culture model by Mina et al. (2017) was more than the distance travelled by cells in the *in silico* model (differences in distances were between 50–100 μm). This could be attributed to the fact that cells tend to move faster in the confined extracellular matrix in a microfluidic device as compared to the unconfined extracellular matrix in other models (Pathak and Kumar, 2012). Additionally, the distance travelled by the simulated cells lies in the range of invasion observed in the experimental models, and supports observations that tumor cells selectively and collectively migrate towards higher concentrations of oxygen (Kenney et al., 2016). The average tumor cell velocity observed in all simulations lies in the physiological range of speeds for tumor cells traveling in 3D hydrogels (Andasari et al., 2018). The increase in tumor cell population in the *in silico* model is ∼4% in the 22% ECM condition regardless of the presence of EndMT-derived activated fibroblasts. The vertical velocity of activated tumor cells decreased with an increase in substrate stiffness from 15% ECM to 75% ECM, but increased at 100% ECM. This could be due to an increase in traction resulting from increased interaction with the surrounding matrix (Lauffenburger and Horwitz, 1996). However, the overall velocity of tumor cells increases with an increase in substrate stiffness. This can be due to the presence of a larger population of non-activated tumor cells than activated cells, thus allowing non-activated tumor cells to influence the overall movement of the cells. As the activation of cells depends on the distance they have travelled, and the cell speeds, the percentage of activated tumor cells also displays a similar biphasic relationship.

The mechanobiology of cancer cell invasion depends on the intra- and extracellular regulation of cell adhesions, protrusions, and tractions. Invasion begins when tumor cells degrade the surrounding tissue through invadopodia, which are actin-rich protrusive structures (Carey et al., 2012a; Parri and Chiarugi, 2010). This degradation occurs via matrix metalloproteinase (MMP)-driven proteolysis (Kumar et al., 2016), and the microtubule and actin cytoskeletons. On a biochemical level, Rho GTPases and the Rac1/WAVE2/Arp2/3 and RhoA/ROCK pathways play a role in tumor invasion, by inducing protrusions and inhibiting actomyosin-dependent contractility (Carey et al., 2012b). When the protrusions are created, integrins on the tumor cell surface attach to ECM ligands and decide the direction in which the tumor should further migrate. This results in a bidirectional signaling network between the ECM and cytoskeleton of the tumor cells, which drives mechanotransduction, molecular switching, and signal transduction, thus playing an important role in cancer progression. This signaling network includes receptor tyrosine kinases, such as focal adhesion kinase (FAK), which control the mechanical and biochemical interactions of the tumor cells with the surrounding tissue (Carey et al., 2012b). Some studies speculate that cytokines secreted by CAFs regulate the remodeling of the actin cytoskeleton through Rho GTPases such as Rac1, RhoA, and Cdc42 (Basquin and Sauvonnet, 2013; Parri and Chiarugi, 2010). This would be a

plausible explanation as to why the presence of cancer-associated fibroblasts increases tumor cell activation and migration. While we see slight differences in tumor cell activation and migration in the two simulated scenarios (i.e. with and without EDAFs), the lack of a clear difference could be because the signaling pathways affected by microenvironmental factors and their resulting cytoskeletal remodeling are not modeled. However, cell-ECM adhesion combined with the degradation of ECM due to MDEs allows cells to preferentially migrate along the ECM cells, i.e. into the extracellular matrix. Thus, while integrin-ligand interactions play a role in cell migration, cytoskeletal remodeling due to CAF-secreted cytokines induces higher tumor cell migration.

The basement membrane is important for maintaining tissue homeostasis, as cells use mechanotransduction to alter their characteristics to respond to ECM properties (Carey et al., 2012b). A study by Alexander et al. (2008) found that the increase in ECM stiffness increased the number and activity of invadopodia through the extracellular signal-receptor kinases (ERK) and FAK and p130Cas signaling molecules. The overactivation of FAK and ERK destabilizes cell-cell adhesions, enhances cell contractility, and regulates transcriptional responses to mechanical signals (Alexander et al., 2008). Tumor invasion also increases through the amplification of integrins and phosphoinositide 3-kinase (PI3K) signaling, which occurs due to the matrix crosslinking that is a result of the stiffening of the tumor microenvironment (Levental et al., 2009; Schrader et al., 2011). Furthermore, β-integrin and FAK are known to regulate tumor cell proliferation in a stiffness-dependent manner (Schrader et al., 2011; Reid et al., 2017). Increased matrix stiffness is also responsible for regulating the STAT3 pathway, which gets activated in response to cytokines and growth factors (Schrader et al., 2011). The conclusions from the simulations align with the molecular and biochemical findings from scientific literature (Fig. 5B). In the computational model, an increase in substrate stiffness causes increased tumor cell-ECM interactions, which results in a higher secretion of MDEs. This in turn, induces more ECM degradation. Along with increased cell migration, this creates more space in the surrounding matrix for tumor cells to multiply, thus resulting in an increase in tumor cell population.

The functional role of EDAFs in a tumor microenvironment differs from cancer-associated fibroblasts (CAFs) derived from other sources as a result of their varied origins. These differences in origin result in varied plasticity, biomarkers, signaling cues, and therapeutic potential (LeBleu and Kalluri, 2018; Tao et al., 2017). For example, EDAFs are positive for biomarkers of alpha-smooth muscle actin (αSMA), fibroblast specific protein-1 (FSP-1), and the endothelial cell-tyrosine kinase receptor Tie2, unlike CAFs derived from epithelial-to-mesenchymal transformation (EMT), resident fibroblasts, or bone marrow (Zeisberg et al., 2007; LeBleu and Kalluri, 2018; Cortez et al., 2014; Okada et al., 1997). These markers allow EndMT-derived activated fibroblasts to exert contractile forces (αSMA) (Marsh et al., 2013) and facilitate malignant progression and recruit macrophages (FSP-1) (Marsh et al., 2013; Park et al., 2016). Moreover, Tie2 are receptors for angiopoietins, which regulate angiogenesis and tumor progression. In addition, the binding initiate several signaling cascades which result in cell differentiation, proliferation, and cell-ECM interactions (Imanishi et al., 2007; Makinde and Agrawal, 2008). To elaborate on the phenomena caused by EDAFs, the next phase of the study will create a more physiologically-relevant stromal tissue by incorporating resident fibroblasts and biochemical factors in the extracellular matrix.

5. Conclusions

The *in silico* model presented here simulates EndMT in a tumor microenvironment, which is related to specific cellular behavior and chemical transport. The cellular mechanobiology observed accurately mimics what is seen *in vitro* tissue models. This work supports the mechanobiological theories of the biochemical signaling pathways which induce the observed behavior and elucidates the biomechanical and biochemical role of EndMT-derived activated fibroblasts in the tumor microenvironment. Coupling the multiscale model with a network model of the underlying signaling pathways can offer insight into the factors that play a significant role in the interactions of EndMT-derived activated fibroblasts with tumor cells as well as the extracellular matrix. Together, it can provide an efficient approach to evaluate the role of EndMT in cancer, facilitate the design further *in vitro* experiments, assess the role of therapeutics, including possible therapy resistance due to the intricate signaling network.

Acknowledgements

The authors would like to gratefully acknowledge Dr. Mei-Hsiu Chen of Statistical Consulting Services at Binghamton University for her suggestions on data presentations.

Funding

This research is supported by the National Science Foundation [grant number CMMI 1436173].

References

Abdulla, T., 2013. *Advances in Modelling of Epithelial to Mesenchymal Transition* (Doctoral). Loughborough University.

Alberts, B., Johnson, A., Lewis, J., Raff, M., Roberts, K., Walter, P., 2002. Molecular Biology of the Cell, 4th ed. Garland Science.

Albro, M.B., Nims, R.J., Cigan, A.D., Yeroushalmi, K.J., Alliston, T., Hung, C.T., Ateshian, G.A., 2013. Accumulation of exogenous activated TGF-β in the superficial zone of articular cartilage. Biophys. J. 104 (8), 1794–1804. https://doi.org/10.1016/j.bpj.2013.02.052.

Alexander, N.R., Branch, K.M., Parekh, A., Clark, E.S., Iwueke, I.C., Guelcher, S.A., Weaver, A.M., 2008. Extracellular matrix rigidity promotes invadopodia activity. Curr. Biol. CB 18 (17), 1295–1299. https://doi.org/10.1016/j.cub.2008.07.090.

An, G., Mi, Q., Dutta-Moscato, J., Vodovotz, Y., 2009. Agent-based models in translational systems biology. Wiley Interdiscip. Rev. Syst. Biol. Med. 1 (2), 159–171. https://doi.org/10.1002/wsbm.45.

Andasari, V., Lü, D., Swat, M., Feng, S., Spill, F., Chen, L., Luo, X., Zaman, M., Long, M., 2018. Computational model of wound healing: EGF secreted by fibroblasts promotes delayed re-epithelialization of epithelial keratinocytes. Integrative Biology 10, 605–634. doi:10.1039/c8ib00048d.

Anderson, A.R.A., 2005. A hybrid mathematical model of solid tumour invasion: the importance of cell adhesion. Math. Med. Biol A J. IMA 22 (2), 163–186. https://doi.org/10.1093/imammb/dqi005.

Anderson, A.R.A., 2007. A hybrid multiscale model of solid tumour growth and invasion: evolution and the microenvironment. In: Anderson, A.R.A., Chaplain, M.A.J., Rejniak, K.A. (Eds.), Single-Cell-Based Models in Biology and Medicine. Birkhäuser Basel, Basel, pp. 3–28.

Arthurs, G.J., Sudhakar, M., 2005. Carbon dioxide transport. Contin. Educ. Anaesth. Crit. Care Pain 5 (6), 207–210. https://doi.org/10.1093/bjaceaccp/mki050.

Bailey, A.M., Lawrence, M.B., Shang, H., Katz, A.J., Peirce, S.M., 2009. Agent-Based model of therapeutic adipose-derived stromal cell trafficking during ischemia predicts ability to roll on P-Selectin. PLoS Comput. Biol. 5 (2), e1000294. https://doi.org/10.1371/journal.pcbi.1000294.

Baker, M., 2015. Mathematical Modelling of Cytokine Dynamics in Arthritic Disease. Nottingham University. Retrieved from http://eprints.nottingham.ac.uk/41497/1/FinalHardboundThesis-MBaker.pdf.

Balter, A., Merks, R.M.H., Popławski, N.J., Swat, M., Glazier, J.A., 2007. The glazier–graner-hogeweg model: extensions, future directions, and opportunities for further study. In: Single-Cell-Based Models in Biology and Medicine. Birkhäuser Basel, pp. 151–167.

Basquin, C., Sauvonnet, N., 2013. Phosphoinositide 3-kinase at the crossroad between endocytosis and signaling of cytokine receptors. Commun. Integr. Biol. 6 (4), e24243. https://doi.org/10.4161/cib.24243.

Belmonte, J.M., Clendenon, S.G., Oliveira, G.M., Swat, M.H., Greene, E.V., Jeyaraman, S., … Bacallao, R.L., 2016. Virtual-tissue computer simulations define the roles of cell adhesion and proliferation in the onset of kidney cystic disease. Mol. Biol. Cell 27 (22), 3673–3685. https://doi.org/10.1091/mbc.e16-01-0059.

Bendas, G., Borsig, L., 2012. Cancer cell adhesion and metastasis: selectins, integrins, and the inhibitory potential of heparins [Research article]. Int J Cell Biol doi:10.1155/2012/676731, 676731.

Caicedo, A., Fritz, V., Brondello, J.-.M., Ayala, M., Dennemont, I., Abdellaoui, N., … Vignais, M.-.L., 2015. MitoCeption as a new tool to assess the effects of mesenchymal stem/stromal cell mitochondria on cancer cell metabolism and function. Sci. Rep. 5, 9073. https://doi.org/10.1038/srep09073.

Carey, S.P., D'Alfonso, T.M., Shin, S.J., Reinhart-King, C.A., 2012a. Mechanobiology of tumor invasion: engineering meets oncology. Crit. Rev. Oncol. Hematol. 83 (2), 170–183. https://doi.org/10.1016/j.critrevonc.2011.11.005.

Carey, S.P., Kraning-Rush, C.M., Williams, R.M., Reinhart-King, C.A., 2012b. Biophysical control of invasive tumor cell behavior by extracellular matrix microarchitecture. Biomaterials 33 (16), 4157–4165. https://doi.org/10.1016/j.biomaterials.2012.02.029.

Cho, J.G., Lee, A., Chang, W., Lee, M.-S., Kim, J., 2018. Endothelial to mesenchymal transition represents a key link in the interaction between inflammation and endothelial dysfunction. Front. Immunol. 9. https://doi.org/10.3389/fimmu.2018.00294.

Cortez, E., Roswall, P., Pietras, K., 2014. Functional subsets of mesenchymal cell types in the tumor microenvironment. Semin. Cancer Biol. 25, 3–9. https://doi.org/10.1016/j.semcancer.2013.12.010.

Cristini, V., Lowengrub, J., 2010. Multiscale Modeling of cancer: an Integrated Experimental and Mathematical Modeling Approach. Cambridge University Press.

Dahal, S., Huang, P., Murray, B.T., Mahler, G.J., 2017. Endothelial to mesenchymal transformation is induced by altered extracellular matrix in aortic valve endothelial cells. J. Biomed. Mater. Res. Part A 105 (10), 2729–2741. https://doi.org/10.1002/jbm.a.36133.

Eladdadi, A., Kim, P., Mallet, D., 2014. Mathematical Models of Tumor-Immune System Dynamics. Springer Proceedings in Mathematics & Statistics, 107. Springer, New York.

Enderling, H., Park, D., Hlatky, L., Hahnfeldt, P., 2009. The importance of spatial distribution of stemness and proliferation state in determining tumor radioresponse. Math. Model. Nat. Phenom. 4 (3), 117–133. https://doi.org/10.1051/mmnp/20094305.

Gerisch, A., Chaplain, M.A.J., 2008. Mathematical modelling of cancer cell invasion of tissue: local and non-local models and the effect of adhesion. J. Theor. Biol. 250 (4), 684–704. https://doi.org/10.1016/j.jtbi.2007.10.026.

Glazier, J.A., Graner, F., 1993. Simulation of the differential adhesion driven rearrangement of biological cells. Phys. Rev. E Stat. Phys. Plasmas Fluids Relat. Interdiscip. Topics 47 (3), 2128–2154.

Gould, R., Bassen, D.M., Chakrabarti, A., Varner, J.D., Butcher, J., 2016. Population heterogeneity in the epithelial to mesenchymal transition is controlled by NFAT and phosphorylated Sp1. PLoS Comput. Biol. 12 (12), e1005251. https://doi.org/10.1371/journal.pcbi.1005251.

Hao, W., Komar, H.M., Hart, P.A., Conwell, D.L., Lesinski, G.B., Friedman, A., 2017. Mathematical model of chronic pancreatitis. Proc. Natl. Acad. Sci. U.S.A. 114 (19), 5011–5016. https://doi.org/10.1073/pnas.1620264114.

Hayflick, L., 1965. The limited in vitro lifetime of human diploid cell strains. Exp. Cell Res. 37, 614–636.

Horsman, M.R., Vaupel, P., 2016. Pathophysiological basis for the formation of the tumor microenvironment. Front. Oncol. 6. https://doi.org/10.3389/fonc.2016.00066.

Hutson, M.S., Leung, M.C.K., Baker, N.C., Spencer, R.M., Knudsen, T.B., 2017. Computational model of secondary palate fusion and disruption. Chem. Res. Toxicol. 30 (4), 965–979. https://doi.org/10.1021/acs.chemrestox.6b00350.

Imanishi, Y., Hu, B., Jarzynka, M.J., Guo, P., Elishaev, E., Bar-Joseph, I., Cheng, S.-Y., 2007. Angiopoietin-2 stimulates breast cancer metastasis through the $\alpha 5\beta 1$ integrin-mediated pathway. Cancer Res. 67 (9), 4254–4263. https://doi.org/10.1158/0008-5472.CAN-06-4100.

Kalli, M., Stylianopoulos, T., 2018. Defining the role of solid stress and matrix stiffness in cancer cell proliferation and metastasis. Front. Oncol. 8. https://doi.org/10.3389/fonc.2018.00055.

Kenney, R.M., Boyce, M.W., Truong, A.S., Bagnell, C.R., Lockett, M.R., 2016. Real-time imaging of cancer cell chemotaxis in paper-based scaffolds. Analyst 141 (2), 661–668. https://doi.org/10.1039/c5an01787d.

Kick, K., Nekolla, K., Rehberg, M., Vollmar, A.M., Zahler, S., 2016. New view on endothelial cell migrationhighlights: switching modes of migration based on matrix composition. Arterioscler. Thromb. Vasc. Biol. 36 (12), 2346–2357. https://doi.org/10.1161/ATVBAHA.116.307870.

Kikuchi, K., Li, X., Zheng, Y., Takano, Y., 2011. Invasion of breast cancer cells into collagen matrix requires TGF-α and Cdc42 signaling. FEBS Lett. 585 (2), 286–290. https://doi.org/10.1016/j.febslet.2010.12.010.

Kleinstreuer, N., Dix, D., Rountree, M., Baker, N., Sipes, N., Reif, D., … Knudsen, T., 2013. A computational model predicting disruption of blood vessel development. PLoS Comput. Biol. 9 (4), e1002996. https://doi.org/10.1371/journal.pcbi.1002996.

Kölsch, V., Charest, P.G., Firtel, R.A., 2008. The regulation of cell motility and chemotaxis by phospholipid signaling. J. Cell. Sci. 121 (Pt 5), 551–559. https://doi.org/10.1242/jcs.023333.

Kumar, S., Kapoor, A., Desai, S., Inamdar, M.M., Sen, S., 2016. Proteolytic and non-proteolytic regulation of collective cell invasion: tuning by ecm density and organization. Sci Rep 6. https://doi.org/10.1038/srep19905.

Lauffenburger, D.A., Horwitz, A.F., 1996. Cell migration: a physically integrated molecular process. Cell 84 (3), 359–369. https://doi.org/10.1016/S0092-8674(00)81280-5.

LeBleu, V.S., Kalluri, R., 2018. A peek into cancer-associated fibroblasts: origins, functions and translational impact. Dis Model Mech 11 (4). https://doi.org/10.1242/dmm.029447.

Lee, H.-O., Silva, A.S., Concilio, S., Li, Y.-S., Slifker, M., Gatenby, R.A., Cheng, J.D., 2011. Evolution of tumor invasiveness: the adaptive tumor microenvironment landscape model. Cancer Res. 71 (20), 6327–6337. https://doi.org/10.1158/0008-5472.CAN-11-0304.

Levental, K.R., Yu, H., Kass, L., Lakins, J.N., Egeblad, M., Erler, J.T., … Weaver, V.M., 2009. Matrix crosslinking forces tumor progression by enhancing integrin signaling. Cell 139 (5), 891–906. https://doi.org/10.1016/j.cell.2009.10.027.

Mahler, G.J., Farrar, E.J., Butcher, J.T., 2013. Inflammatory cytokines promote mesenchymal transformation in embryonic and adult valve endothelial cells. Arterioscler. Thromb. Vasc. Biol. 33 (1), 121–130. https://doi.org/10.1161/ATVBAHA.112.300504.

Makinde, T., Agrawal, D.K., 2008. Intra and extravascular transmembrane signalling of angiopoietin-1-Tie2 receptor in health and disease. J. Cell. Mol. Med. 12 (3), 810–828. https://doi.org/10.1111/j.1582-4934.2008.00254.x.

Mandel, K., Seidl, D., Rades, D., Lehnert, H., Gieseler, F., Hass, R., Ungefroren, H., 2013. Characterization of spontaneous and TGF-β-Induced cell motility of primary human normal and neoplastic mammary cells in vitro using novel real-time technology. PLoS ONE 8 (2), e56591. https://doi.org/10.1371/journal.pone.0056591.

Marin-Riera, M., Brun-Usan, M., Zimm, R., Välikangas, T., Salazar-Ciudad, I., 2016. Computational modeling of development by epithelia, mesenchyme and their interactions: a unified model. Bioinformatics 32 (2), 219–225. https://doi.org/10.1093/bioinformatics/btv527.

Markwalder, T.-M., Grolimund, P., Seiler, R.W., Roth, F., Aaslid, R., 1984. Dependency of blood flow velocity in the middle cerebral artery on end-tidal carbon dioxide partial pressure—a transcranial ultrasound doppler study. J. Cereb. Blood Flow Metab. 4 (3), 368–372. https://doi.org/10.1038/jcbfm.1984.54.

Marsh, T., Pietras, K., McAllister, S.S., 2013. Fibroblasts as architects of cancer pathogenesis. Biochim. Biophys. Acta 1832 (7), 1070–1078. https://doi.org/10.1016/j.bbadis.2012.10.013.

McKeown, S.R., 2014. Defining normoxia, physoxia and hypoxia in tumours-implications for treatment response. Br. J. Radiol. 87 (1035), 20130676. https://doi.org/10.1259/bjr.20130676.

Mina, S.G., Huang, P., Murray, B.T., Mahler, G.J., 2017. The role of shear stress and altered tissue properties on endothelial to mesenchymal transformation and tumor-endothelial cell interaction. Biomicrofluidics 11 (4), 044104. https://doi.org/10.1063/1.4991738.

Mosadegh, B., Lockett, M.R., Minn, K.T., Simon, K.A., Gilbert, K., Hillier, S., … Whitesides, G.M., 2015. A paper-based invasion assay: assessing chemotaxis of cancer cells in gradients of oxygen. Biomaterials 52, 262–271. https://doi.org/10.1016/j.biomaterials.2015.02.012.

Nargis, N.N., Aldredge, R.C., Guy, R.D., 2018. The influence of soluble fragments of extracellular matrix (ECM) on tumor growth and morphology. Math. Biosci. 296, 1–16. https://doi.org/10.1016/j.mbs.2017.11.014.

Neagu, A., Mironov, V., Kosztin, I., Barz, B., Neagu, M., Moreno-Rodriguez, R.A., Forgacs, G., 2010. Computational modeling of epithelial–mesenchymal transformations. Biosystems 100 (1), 23–30. https://doi.org/10.1016/j.biosystems.2009.12.004.

Oden, J.T., Lima, E.A.B.F., Almeida, R.C., Feng, Y., Rylander, M.N., Fuentes, D., … Zhou, J.C., 2016. Toward predictive multiscale modeling of vascular tumor growth: computational and experimental oncology for tumor prediction. Arch. Comput. Methods Eng. 23 (4), 735–779. https://doi.org/10.1007/s11831-015-9156-x.

Okada, H., Danoff, T.M., Kalluri, R., Neilson, E.G., 1997. Early role of Fsp1 in epithelial-mesenchymal transformation. Am. J. Physiol. 273 (4 Pt 2), F563–F574.

Pardali, E., Sanchez-Duffhues, G., Gomez-Puerto, M.C., ten Dijke, P., 2017. TGF-β-Induced endothelial-mesenchymal transition in fibrotic diseases. Int. J. Mol. Sci. 18 (10). https://doi.org/10.3390/ijms18102157.

Park, C.K., Jung, W.H., Koo, J.S., 2016. Expression of cancer-associated fibroblast-related proteins differs between invasive lobular carcinoma and invasive ductal carcinoma. Breast Cancer Res. Treat. 159 (1), 55–69. https://doi.org/10.1007/s10549-016-3929-2.

Parri, M., Chiarugi, P., 2010. Rac and Rho GTPases in cancer cell motility control. Cell Commun. Signal. CCS 8, 23. https://doi.org/10.1186/1478-811X-8-23.

Pathak, A., Kumar, S., 2012. Independent regulation of tumor cell migration by matrix stiffness and confinement. Proc. Natl. Acad. Sci. U.S.A. 109 (26), 10334–10339. https://doi.org/10.1073/pnas.1118073109.

Pérez, L., Muñoz-Durango, N., Riedel, C.A., Echeverría, C., Kalergis, A.M., Cabello-Verrugio, C., Simon, F., 2017. Endothelial-to-mesenchymal transition: cytokine-mediated pathways that determine endothelial fibrosis under inflammatory conditions. Cytokine Growth Factor Rev. 33, 41–54. https://doi.org/10.1016/j.cytogfr.2016.09.002.

Popel, A.S., 1989. Theory of oxygen transport to tissue. Crit. Rev. Biomed. Eng. 17 (3), 257–321.

Popławski, N.J., Agero, U., Gens, J.S., Swat, M., Glazier, J.A., Anderson, A.R.A., 2009. Front instabilities and invasiveness of simulated avascular tumors. Bull. Math. Biol. 71 (5), 1189–1227. https://doi.org/10.1007/s11538-009-9399-5.

Potenta, S., Zeisberg, E., Kalluri, R., 2008. The role of endothelial-to-mesenchymal transition in cancer progression. Br. J. Cancer 99 (9), 1375–1379. https://doi.org/10.1038/sj.bjc.6604662.

Ramis-Conde, I., Chaplain, M.A.J., Anderson, A.R.A., 2008. Mathematical modelling of cancer cell invasion of tissue. Math. Comput. Model. 47 (5–6), 533–545. https://doi.org/10.1016/j.mcm.2007.02.034.

Reid, S.E., Kay, E.J., Neilson, L.J., Henze, A.-T., Serneels, J., McGhee, E.J., … Zanivan, S., 2017. Tumor matrix stiffness promotes metastatic cancer cell interaction with the endothelium. EMBO J., e201694912. https://doi.org/10.15252/embj.201694912.

Rejniak, K.A., Anderson, A.R.A., 2011. Hybrid models of tumor growth. Wiley Interdiscip. Rev. Syst. Biol. Med. 3 (1), 115–125. https://doi.org/10.1002/wsbm.102.

Roussos, E.T., Condeelis, J.S., Patsialou, A., 2011. Chemotaxis in cancer. Nat. Rev. Cancer 11 (8), 573–587. https://doi.org/10.1038/nrc3078.

Rubin, H., 2002. The disparity between human cell senescence *in vitro* and lifelong replication *in vivo*. Nat. Biotechnol. 20 (7), 675–681. https://doi.org/10.1038/nbt0702-675.

Sai, J., Rogers, M., Hockemeyer, K., Wikswo, J.P., Richmond, A., 2016. Study of chemotaxis and cell–cell interactions in cancer with microfluidic devices. Meth. Enzymol. 570, 19–45. https://doi.org/10.1016/bs.mie.2015.09.023.

Saito, A., 2013. EMT and EndMT: regulated in similar ways? J. Biochem. 153 (6), 493–495. https://doi.org/10.1093/jb/mvt032.

Schrader, J., Gordon-Walker, T.T., Aucott, R.L., van Deemter, M., Quaas, A., Walsh, S., … Iredale, J.P., 2011. Matrix stiffness modulates proliferation, chemotherapeutic response and dormancy in hepatocellular carcinoma cells. Hepatology (Baltimore, Md.) 53 (4), 1192–1205. https://doi.org/10.1002/hep.24108.

Shirinifard, A., Gens, J.S., Zaitlen, B.L., Popławski, N.J., Swat, M., Glazier, J.A., 2009. 3D Multi-Cell simulation of tumor growth and angiogenesis. PLoS ONE 4 (10), e7190. https://doi.org/10.1371/journal.pone.0007190.

Sluka, J.P., Fu, X., Swat, M., Belmonte, J.M., Cosmanescu, A., Clendenon, S.G., … Glazier, J.A., 2016. A liver-centric multiscale modeling framework for xenobiotics. PLoS ONE 11 (9), e0162428. https://doi.org/10.1371/journal.pone.0162428.

Su, B., Zhou, W., Dorman, K.S., Jones, D.E., 2009. Mathematical modelling of immune response in tissues. Comput. Math. Method. Med. 10 (1), 9–38. https://doi.org/10.1080/17486700801982713.

Swat, M.H., Thomas, G.L., Belmonte, J.M., Shirinifard, A., Hmeljak, D., Glazier, J.A., 2012. Multi-Scale modeling of tissues using CompuCell3D. Method. Cell. Biol. 110, 325–366. https://doi.org/10.1016/B978-0-12-388403-9.00013-8.

Swat, M.H., Shirinifard, A., Balter, A., Popławski, N.J., Glazier, J.A. 2013. *CompuCell3D quick start guide version 3.7.0.* Retrieved from http://www.compucell3d.org/BinDoc/cc3d_binaries/Manuals/PASI_compucell3d_quickstartguide_2.0.pdf.

Swat, M.H., Thomas, G.L., Shirinifard, A., Clendenon, S.G., Glazier, J.A., 2015. Emergent stratification in solid tumors selects for reduced cohesion of tumor cells: a multi-cell, virtual-tissue model of tumor evolution using compucell3d. PLoS ONE 10 (6), e0127972. https://doi.org/10.1371/journal.pone.0127972.

Szabó, A., Merks, R.M.H., 2013. Cellular potts modeling of tumor growth, tumor invasion, and tumor evolution. Front Oncol 3. https://doi.org/10.3389/fonc.2013.00087.

Szot, C.S., Buchanan, C.F., Rylander, M.N., Freeman, J.W., 2011. Cancer cells cultured within collagen I hydrogels exhibit an *in vivo* solid tumor phenotype. In: 2011 IEEE 37th Annual Northeast Bioengineering Conference (NEBEC), pp. 1–2.

Tang, L., Ven, A.L., Guo, D., Andasari, V., Cristini, V., Li, K.C., Zhou, X., 2014. Computational modeling of 3D tumor growth and angiogenesis for chemotherapy evaluation. PLoS ONE 9 (1), e83962. https://doi.org/10.1371/journal.pone.0083962.

Tao, L., Huang, G., Song, H., Chen, Y., Chen, L., 2017. Cancer associated fibroblasts: an essential role in the tumor microenvironment. Oncol Lett 14 (3), 2611–2620. https://doi.org/10.3892/ol.2017.6497.

Trepiana, J., Meijide, S., Navarro, R., Hernández, M.L., Ruiz-Sanz, J.I., Ruiz-Larrea, M.B., 2017. Influence of oxygen partial pressure on the characteristics of human hepatocarcinoma cells. Redox. Biol. 12, 103–113. https://doi.org/10.1016/j.redox.2017.02.004.

Truong, D., Puleo, J., Llave, A., Mouneimne, G., Kamm, R.D., Nikkhah, M., 2016. Breast cancer cell invasion into a three dimensional tumor-stroma microenvironment. Sci. Rep. 6, 34094. https://doi.org/10.1038/srep34094.

Usselman, R.J., Chavarriaga, C., Castello, P.R., Procopio, M., Ritz, T., Dratz, E.A., … Martino, C.F., 2016. The quantum biology of reactive oxygen species partitioning impacts cellular bioenergetics. Sci. Rep. 6, 38543. https://doi.org/10.1038/srep38543.

Virgilio, K.M., Martin, K.S., Peirce, S.M., Blemker, S.S., 2015. Multiscale models of skeletal muscle reveal the complex effects of muscular dystrophy on tissue mechanics and damage susceptibility. Interf. Focus 5 (2), 20140080. https://doi.org/10.1098/rsfs.2014.0080.

Wagner, B.A., Venkataraman, S., Buettner, G.R., 2011. The rate of oxygen utilization by cells. Free Radic. Biol. Med. 51 (3). 700–712 https://doi.org/10.1016/j.freeradbiomed.2011.05.024 .

Wang, X., Ali, M.S., Lacerda, C.M.R., 2018. A three-dimensional collagen-elastin scaffold for heart valve tissue engineering. Bioengineering (Basel, Switzerland) 5 (3). https://doi.org/10.3390/bioengineering5030069.

Wen, J.H., Choi, O., Taylor-Weiner, H., Fuhrmann, A., Karpiak, J.V., Almutairi, A., Engler, A.J., 2015. Haptotaxis is cell type specific and limited by substrate adhesiveness. Cell. Mol. Bioeng. 8 (4), 530–542. https://doi.org/10.1007/s12195-015-0398-3.

Yeon, J.H., Jeong, H.E., Seo, H., Cho, S., Kim, K., Na, D., … Kang, J.Y., 2018. Cancer-derived exosomes trigger endothelial to mesenchymal transition followed by the induction of cancer-associated fibroblasts. Acta Biomater. 76, 146–153. https://doi.org/10.1016/j.actbio.2018.07.001.

Yu, J., Tian, S., Metheny-Barlow, L., Chew, L.-J., Hayes, A.J., Pan, H., … Li, L.-Y., 2001. Modulation of endothelial cell growth arrest and apoptosis by vascular endothelial growth inhibitor. Circ. Res. 89 (12), 1161–1167. https://doi.org/10.1161/hh2401.101909.

Zeisberg, E.M., Potenta, S., Xie, L., Zeisberg, M., Kalluri, R., 2007. Discovery of endothelial to mesenchymal transition as a source for carcinoma-associated fibroblasts. Cancer Res. 67 (21), 10123–10128. https://doi.org/10.1158/0008-5472.CAN-07-3127.